An Adaptive Change Threshold Selection Method Based on Land Cover Posterior Probability and Spatial Neighborhood Information

Huaqiao Xing, Linye Zhu, Yongyu Feng, Wei Wang, Dongyang Hou, Fei Meng, and Yuanlong Ni

***Abstract*—Change threshold selection (CTS) plays an important role in land cover change detection. The traditional CTS methods are mainly based on the information contained in grayscale histogram distributions or pixel neighborhoods. However, land cover is highly spatially heterogeneous, and changes in different land cover types are characterized by different magnitudes. Unfortunately, few CTS studies have considered the effects of both land cover type and spatial heterogeneity on CTS, potentially leading to false alarms or missed alarms. To address this challenge, we propose an adaptive CTS method based on land cover posterior probability and spatial neighborhood information (LCSN). First, the posterior probability of the change magnitude in each land cover type is calculated according to a Bayesian criterion to integrate the land cover type information. Second, the posterior probability is calculated using a bilateral filtering method to construct the spatial surface based on the land cover type and spatial neighborhood information. Finally, the degree of difference between the spatial surface and the change magnitude map is taken as the final threshold. The proposed LCSN method is verified with Landsat 8-Operational Land Imager images and IKONOS images. The experimental results show that the LCSN method is effective in reducing the pseudo changes and identifying changes in land cover types with low grayscale values in the corresponding change magnitude maps.**

***Index Terms*—Bilateral filtering, change detection, class probability, threshold selection.**

Manuscript received July 12, 2021; revised September 9, 2021 and September 26, 2021; accepted October 27, 2021. Date of publication November 2, 2021; date of current version November 24, 2021. This work was supported in part by the National Natural Science Foundation of China under Grant 41801308, in part by the Key Laboratory of Land Satellite Remote Sensing Application Center, Ministry of Natural Resources of the People's Republic of China under Grant KLSMNR-202105, in part by the Doctoral Research Fund of Shandong Jianzhu University under Grant XNBS1804, and in part by the Open Fund of State Laboratory of Information Engineering in Surveying, Mapping and Remote Sensing, Wuhan University under Grant 20S01. *(Corresponding authors: Linye Zhu; Wei Wang.)*

Huaqiao Xing, Linye Zhu, and Fei Meng are with the School of Surveying and Geo-Informatics, Shandong Jianzhu University, Jinan 250101, China (e-mail: xinghuaqiao@126.com; 895916547@qq.com; lzhmf@sdjzu.edu.cn).

Yongyu Feng and Yuanlong Ni are with the Shandong Institute of Territorial Spatial Data and Remote Sensing Technology, Jinan 250014, China (e-mail: fengyongyu@shandong.cn; 729833504@qq.com).

Wei Wang is with the National Disaster Reduction Center of China, Beijing 100124, China (e-mail: wangwei@ndrcc.gov.cn).

Dongyang Hou is with the School of Geosciences and Info Physics, Central South University, Changsha 410083, China (e-mail: houdongyang1986@cumt.edu.cn).

Digital Object Identifier 10.1109/JSTARS.2021.3124491

I. Introduction

MULTITEMPORAL remote sensing change detection has played an increasingly vital role in the fields of natural resource management, environmental protection, land cover dynamic monitoring, etc., [1]–[3]. Change threshold selection (CTS) is an essential step that directly affects the detection results [4]–[7].

The selection of change thresholds, as a relatively complex process, is jointly influenced by multiple factors. Various land cover types possess different change magnitudes in change detection [8]. For instance, the spectral change values for grassland and woodland are relatively small, but those for farmland converted to building land are relatively large [9]. In addition, different land covers exhibit different spatial heterogeneity depending on the study area and the resolution of the remote sensing images considered [10], [11]. For example, spatial heterogeneity decreases when the study area is filled with farmland. All these factors contribute to the difficulty of CTS.

Various CTS approaches have emerged in the past three decades and can be classified into global and local CTS methods. Global CTS methods are usually based on the grayscale histogram distribution and divide the corresponding change magnitude map (CMM) into changed and unchanged areas based on one or more indicators [12]–[14]. Some classical methods include the Otsu method [15], Kapur method [16], Kittler method [17], and expectation maximum (EM) method [18]. As a recent example, Cui *et al.* [19] proposed a dual-threshold SAR change detection method combined with normalized maximum interclass variance and the generalized Kittler and Illingworth thresholding method. Although convenient and efficient, global CTS methods holistically lack consideration of land cover types and spatial heterogeneity. Local CTS methods generally set a suitable window size (e.g., 3×3) to divide a CMM into subregions of the same size and perform threshold segmentation within the subregions [20]–[22]. For example, Yang *et al.* [23] proposed a variable class fuzzy threshold optical remote sensing image segmentation method based on local spatial information, which is applicable to multi-threshold segmentation of remote sensing images. This approach considers spatial heterogeneity to some degree without integrating land cover types. It is worth noting that if the differences in spectral changes among land cover types are ignored, the determination of thresholds will produce false alarm and missed alarm problems [24]. In recent years,

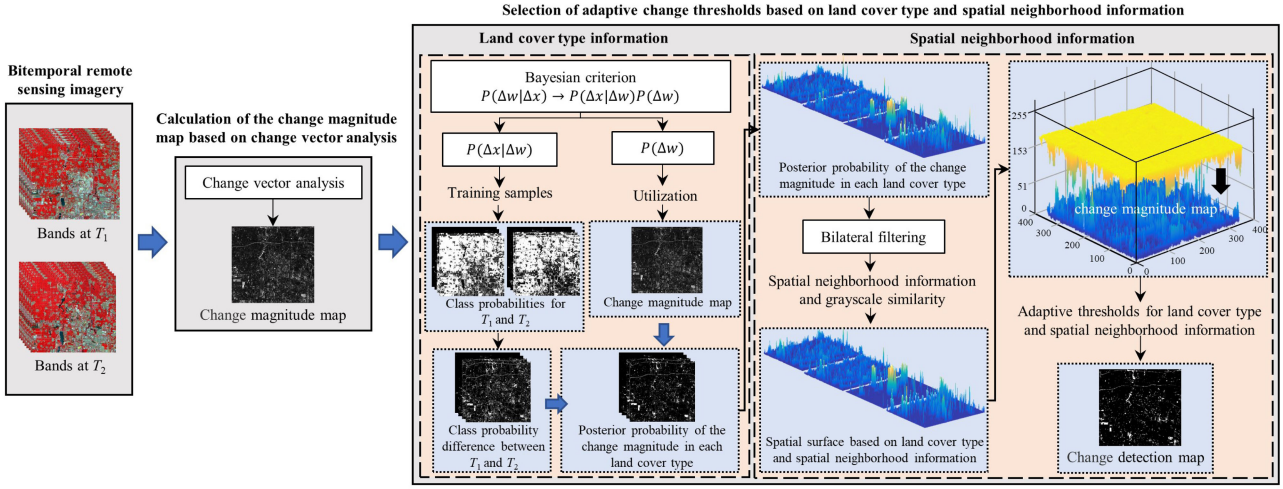

Fig. 1. Flowchart of the LCSN method.

some scholars have introduced land cover type information into CTS. For example, Xian *et al.* [25] used the mean and variance of change vectors and artificially set adjustment coefficients to determine thresholds for different land cover types. Liu and Zhang [9] proposed using the maximum interclass variance method to determine change thresholds for different land cover types. The above-mentioned approaches enhanced the universality and stability of CTS, yet the consideration of spatial heterogeneity remains insufficient and cannot effectively address the problem of CTS for complex land cover types. Consequently, accounting for land cover types and spatial heterogeneity is necessary for improving the generality of CTS.

To solve the above problems, an adaptive CTS method based on land cover posterior probability and spatial neighborhood information (LCSN) is proposed. First, the posterior probability of the change magnitude in each land cover type is measured based on a Bayesian criterion to obtain the land cover type information. Second, the spatial surface based on land cover type and spatial neighborhood information is constructed by integrating the associated spatial neighborhood information in the posterior probability using a bilateral filtering (BF) method. Finally, the final adaptive threshold for each pixel of the CMM is determined by the degree of difference between the spatial surface and the CMM.

The main contribution and innovation of our work is the integration of land cover type and spatial neighborhood information for adaptive CTS, which improves the distinguishability of changed and unchanged areas. The posterior probability and BF approach are used to construct spatial surface of change threshold. The specific threshold could be calculated according to the feature of land cover type and spatial neighborhood in each pixel. The proposed LCSN method can effectively reduce pseudo changes, and identify real changes with lower grayscale values in the CMM, which minimizes the possibility of missed and false alarms.

The rest of this article is organized as follows. Section II introduces the LCSN method. Section III provides a comparative analysis of the proposed method and traditional methods based on remote sensing images. Finally, Section IV further discusses the LCSN method. Section V concludes this article.

II. Methodology

The framework of the specific change detection process is given in Fig. 1. First, the CMM is determined from bitemporal remote sensing images using change vector analysis (CVA). Second, the posterior probability of the change magnitude in each land cover type is derived according to a Bayesian criterion. Then, the BF method is employed to obtain spatial neighborhood information for the posterior probability and construct an adaptive spatial surface based on land cover type and spatial neighborhood information. Finally, the final threshold is obtained from the difference degree between the spatial surface and the CMM.

A. Calculation of the CMM Based on Change Vector Analysis

In multitemporal change detection, the grayscale level vectors of image pixels at moments T_1 and T_2 are $G = (g_1, g_2, \ldots, g_k)^T$ and $H = (h_1, h_2, \ldots, h_k)^T$, respectively. ΔG contains all the change information in both images, and the change magnitude is determined by $\|\Delta G\|$. The specific CVA equations are as follows [26], [27]:

$$\Delta G = G - H = \begin{pmatrix} g_1 - h_1 \\ g_2 - h_2 \\ \cdots \\ g_k - h_k \end{pmatrix} \tag{1}$$

$$\|\Delta G\| = \sqrt{(g_1 - h_1)^2 + (g_2 - h_2)^2 + \ldots + (g_k - h_k)^2} \tag{2}$$

where k denotes the kth band, and g_k and h_k denote the grayscale level of each band in time periods T_1 and T_2, respectively.

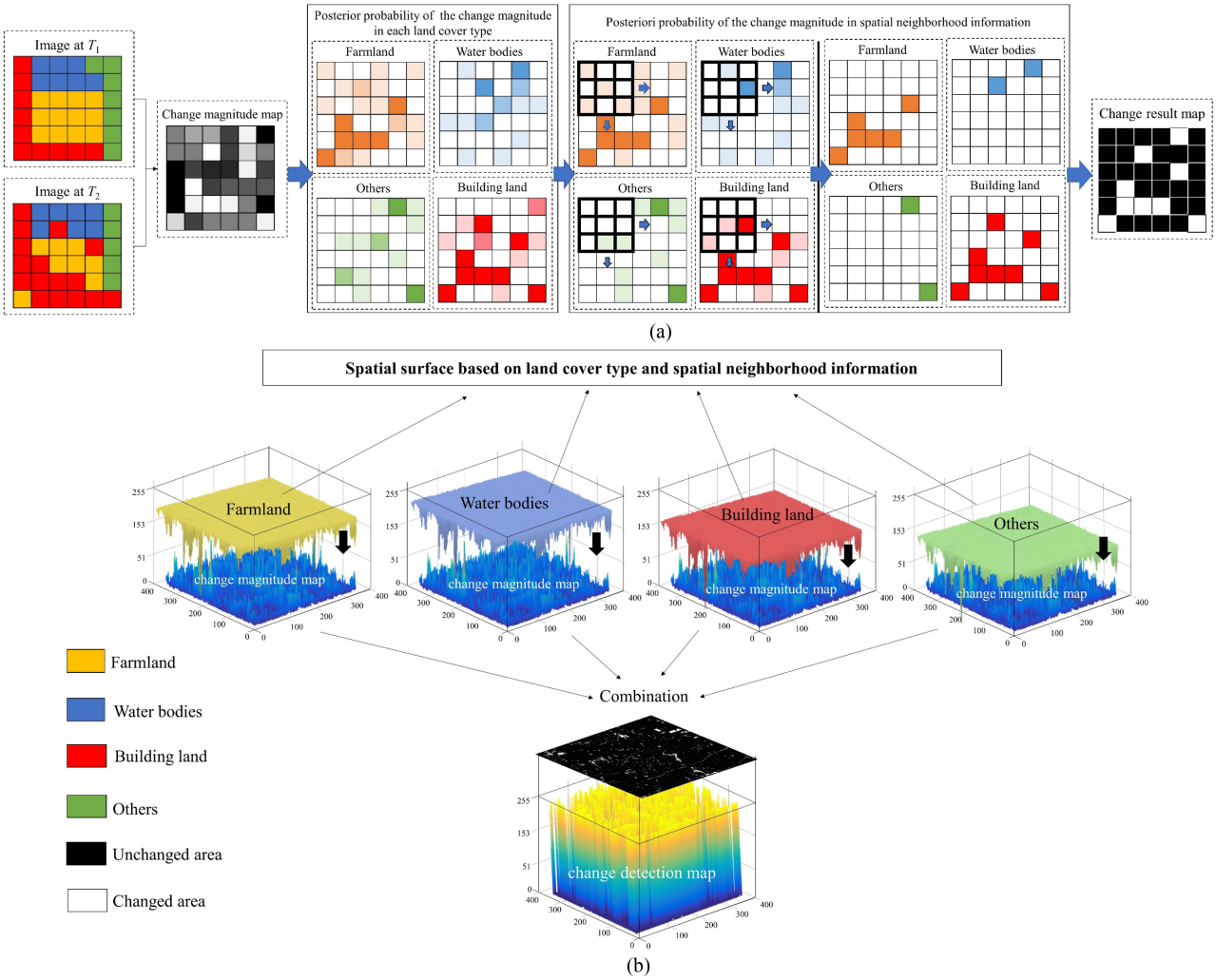

Fig. 2. Theoretical map of the LCSN method. (a) 2-D principle. (b) 3-D principle.

B. Selection of Adaptive Change Thresholds Based on Land Cover Type and Spatial Neighborhood Information

A three-dimensional (3-D) Cartesian coordinate system is established to incorporate the CMM into 3-D space with (x, y, z) coordinates, where x and y represent the horizontal and vertical coordinates of the pixel points in the CMM and z is the change magnitude of the pixel points normalized to 0–255. The spatial surface based on land cover type and spatial neighborhood information is developed based on a Bayesian criterion and the BF method, as shown in Fig. 2. Considering the different magnitudes of land cover type changes when selecting the threshold value, the posterior probability of the change magnitude in each land cover type can avoid the omission of land cover type changes with smaller magnitude. On this basis, the spatial neighborhood information of the posterior probability is considered to further increase the spatial surface value of the possible changed areas and weaken the spatial surface value of the possible unchanged areas.

According to Bayesian theory, it is assumed that the spectral change at a given moment is Δx in the bitemporal remote sensing image, and the corresponding change in land cover type is Δw. The posterior probability of the change magnitude based on land cover type information is as follows [28], [29]:

$$P\ (\Delta w|\Delta x) = \frac{P(\Delta x|\Delta w)P\ (\Delta w)}{P\ (\Delta x)} \ \rightarrow P(\Delta x|\Delta w)P\ (\Delta w) \tag{3}$$

$$P\ (\Delta x|\Delta w) = \left|p\left(w_{i_{T_2}}\right) - p\left(w_{i_{T_1}}\right)\right| \tag{4}$$

where $P(\Delta x)$ is independent of the land cover type and does not contribute to the determination of the posterior probability; $P(\Delta w)$ is the CVA-based CMM, i is the land cover type at moments T_1 and T_2, $p(w_{i_{T_1}})$ and $p(w_{i_{T_2}})$ are the class probabilities at moments T_1 and T_2, respectively, obtained through a support vector machine [30], [31], and $P(\Delta x|\Delta w)$ is the difference between the class probabilities at moments T_1 and T_2.

The spatial neighborhood information is obtained using the BF method for the posterior probability of the change magnitude in each land cover type. The BF method is a nonlinear filtering

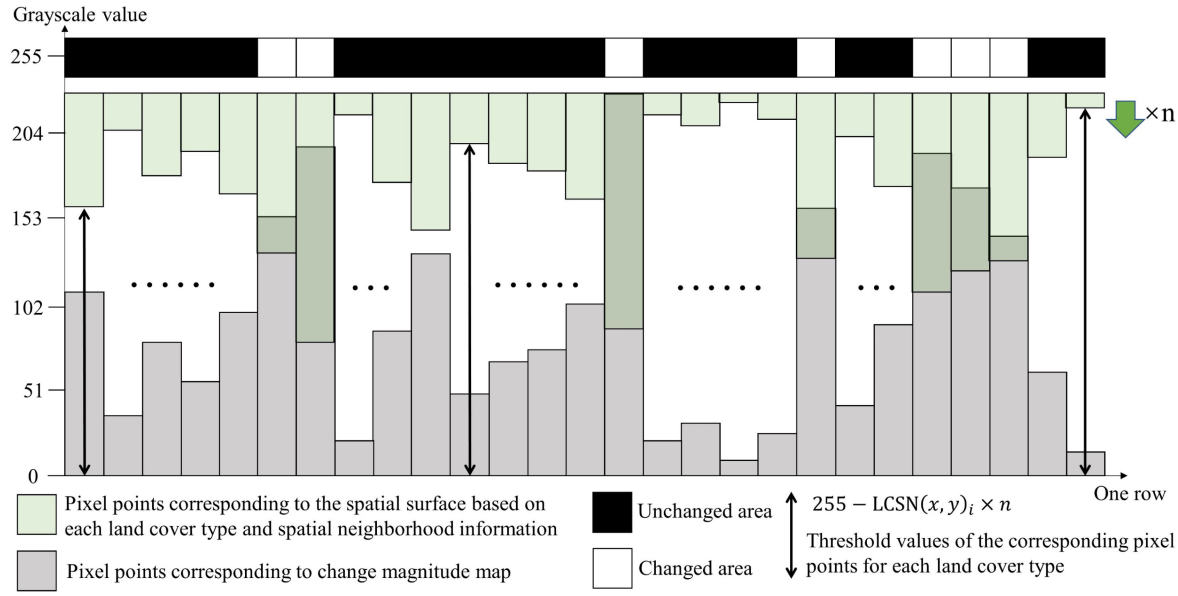

Fig. 3. Principle of threshold judgment in one row of the CMM.

method that achieves a compromise between spatial proximity and the similarity of pixel values considering both spatial neighborhood information and grayscale similarity for the purpose of edge-preserving denoising [32], [33]

$$X[k] = \frac{\sum_{n=-N}^{N} W[k,n]\, Y[k-n]}{\sum_{n=-N}^{N} W[k,n]} \tag{5}$$

$$W[k,n] = W_S[k,n] \cdot W_R[k,n] \tag{6}$$

$$W_S[k,n] = \exp\left\{-\frac{d^2\{[k],[k-n]\}}{2\sigma_S^2}\right\} = \exp\left\{-\frac{n^2}{2\sigma_S^2}\right\} \tag{7}$$

$$W_R[k,n] = \exp\left\{-\frac{d^2\{Y[k],Y[k-n]\}}{2\sigma_R^2}\right\} = \exp\left\{-\frac{[Y[k]-Y[k-n]]^2}{2\sigma_R^2}\right\} \tag{8}$$

where $X[k]$ is the normalized weighted average of the $[2N+1]$ sample neighborhood around the kth sample, the weights $W[k,n]$ are calculated from the information in the neighborhood, $X[k]$ is the central sample, $W_S[k,n]$ is the spatial weight of the image, measuring the Euclidean metric geometric distance between the central sample $[k]$ and the $[k-n]$ samples, $W_R[k,n]$ is the radiometric weight, measuring the Euclidean metric radiometric distance between the central sample $Y[k]$ and the samples $Y[k-n]$, N is the filter support variable, and σ_S and σ_R are parameters that control the attenuation of the weighting factors.

The adaptive thresholds are mainly determined by the degree of difference between the spatial surface based on land cover type and spatial neighborhood information and the CMM. As shown in Fig. 3, in the constructed spatial surface (green squares), there are larger values for possible changed areas and relatively smaller values for possible unchanged areas. Because the CMM is standardized to 0–255, the final threshold value is equal to 255 minus the spatial surface based on land cover type and spatial neighborhood information multiplied by the coefficient n. Higher gray squares indicate a high likelihood of change, and vice versa. The LCSN method establishes small thresholds for areas of possible change in the CMM and large thresholds for areas unlikely to change to reduce the possibility of detecting pseudo changes. Thus, the LCSN method effectively distinguishes between changed and unchanged areas and increases the degree of adaptiveness in CTS.

$$\mathrm{CMM} = \begin{cases} \text{change}, & \mathrm{CMM}(x,y) \geq 255 - \mathrm{LCSN}(x,y)_i \times n \\ \text{no\_change}, & \mathrm{CMM}(x,y) < 255 - \mathrm{LCSN}(x,y)_i \times n \end{cases} \tag{9}$$

where $\mathrm{CMM}(x,y)$ is the pixel value corresponding to the CMM, i is the land cover type, $\mathrm{LCSN}(x,y)$ is the spatial surface based on land cover type and spatial neighborhood information, and n is a coefficient used to improve the distinguishability of thresholds.

III. Experimental Results and Analysis

To demonstrate the effectiveness of the LCSN method, a comparative analysis was conducted with seven CTS methods based on Landsat 8-Operational Land Imager (OLI) images and IKONOS high-resolution images. These methods include global CTS methods (the Otsu method, Kittler method, and EM method), local CTS methods (the active contour method [34], Bernsen method [35], and Niblack method [36]), and the LCT method. The LCT method uses the posterior probability of the change magnitude in each land cover type as the CMM, and

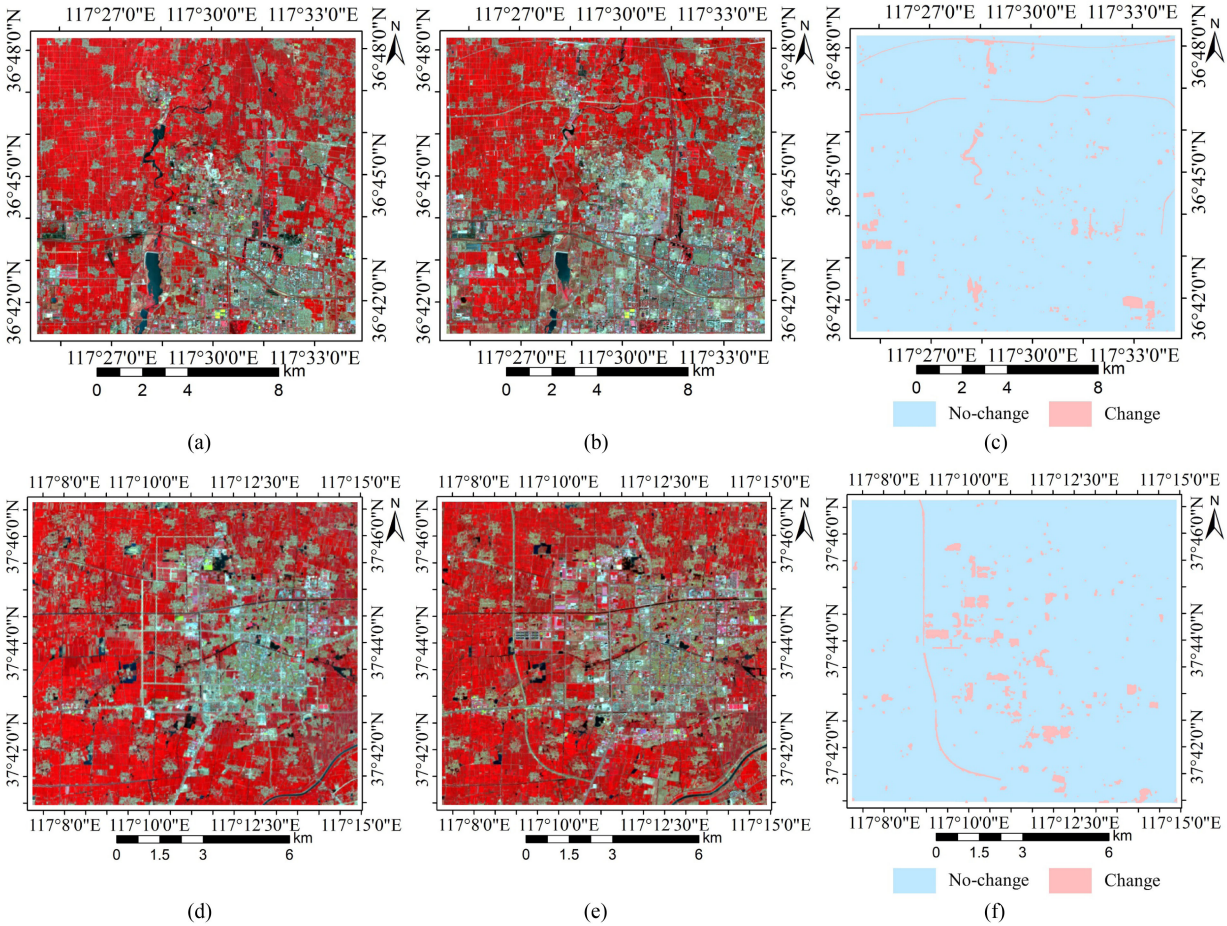

Fig. 4. (a) and (b) Remote sensing images of study area A in 2013 and 2018, respectively. (c) Reference map for study area A. (d) and (e) Remote sensing images of study area B in 2013 and 2018, respectively. (f) Reference map for study area B.

selects the threshold value using the EM method. The overall accuracy (OA), kappa coefficient (κ), omission rate (OR), commission rate (CR), and F_1-score were used to evaluate the change detection results.

A. *Experiments in Study Area A and Study Area B Using Landsat 8 Data*

The study areas were photographed on May 21, 2013, and May 3, 2018, as Landsat 8-OLI images at a 30-m resolution with coastal, red, green, blue, near-infrared, SWIR 1, and SWIR 2 bands. Study area A is located in Jinan City, Shandong Province, China, with an image size of 467×434 pixels. The image size of study area B is 376×350 pixels, and this area covers Leling City, Shandong Province, China. The study areas are characterized by varying degrees of surface variability (see Fig. 4). The study areas were preprocessed with radiometric calibration, atmospheric correction and geometric correction [37], [38]. The land types in the study area were classified as farmland, water bodies, building land, etc. Training samples corresponding to the land cover types in the bitemporal remote sensing images were chosen to compute the class probabilities for the study area [39], [40].

The expansion of roads and building land and shrinkage of water bodies occurred in study area A from 2013 to 2018, and study area B experienced growth in roads and building land. The black area in the change detection results is the unchanged area, and the white area is the changed area. We selected 1181 samples of pixels with change and 3326 samples of pixels without change from study area A, as well as 1471 and 1145 corresponding samples from study area B, respectively, for accuracy assessment, as shown in Tables I and II.

The results of the quantitative accuracy assessment indicate that the global CTS methods (e.g., OTSU, Kittler, and EM) yield notable false alarms. The local CTS methods reduce false alarms to some extent but also produce missed alarms, which was particularly evident for the Bernsen method. The LCT method mainly suffers from false alarm issues. Based on OA, κ, and F_1-score, the LCSN method achieves the highest accuracy in both study areas with the OA greater than 90%. Compared to other CTS methods, the LCSN method is closest to simulating the real change results (see Figs. 5 and 6).

The LCSN method is compared with the unsupervised CTS method and the supervised CTS method. The unsupervised CTS method is based on global and spatial neighborhood

TABLE I
COMPARISON OF THE ACCURACY OF THE EIGHT CTS METHODS FOR STUDY AREA A

Method	Unsupervised						Supervised	
	Global			Spatial neighborhood information			Land cover type information	Land cover type and spatial neighborhood information
	OTSU	Kittler	EM	Active contour	Bernsen	Niblack	LCT	**LCSN**
OA (%)	79.36	73.24	71.02	73.19	82.62	88.97	87.04	**91.10**
κ	0.57	0.47	0.44	0.47	0.56	0.74	0.70	**0.79**
CR (%)	27.78	36.20	39.27	35.96	13.08	13.32	17.08	**11.27**
OR (%)	0.51	0.17	0.00	1.02	29.47	4.57	1.35	**2.20**
F_1-score (%)	71.64	66.16	64.39	65.93	68.02	81.93	79.95	**85.20**

TABLE II
COMPARISON OF THE ACCURACY OF THE EIGHT CTS METHODS FOR STUDY AREA B

Method	Unsupervised						Supervised	
	Global			Spatial neighborhood information			Land cover type information	Land cover type and spatial neighborhood information
	OTSU	Kittler	EM	Active contour	Bernsen	Niblack	LCT	**LCSN**
OA (%)	83.86	83.86	82.22	84.74	63.57	84.05	89.48	**91.62**
κ	0.65	0.65	0.62	0.67	0.28	0.66	0.78	**0.82**
CR (%)	35.11	35.11	40.44	32.14	24.37	29.26	23.58	**18.52**
OR (%)	1.36	1.36	0.14	2.11	45.82	5.57	0.34	**0.48**
F_1-score (%)	87.30	87.30	86.33	87.83	62.58	86.94	91.42	**93.04**

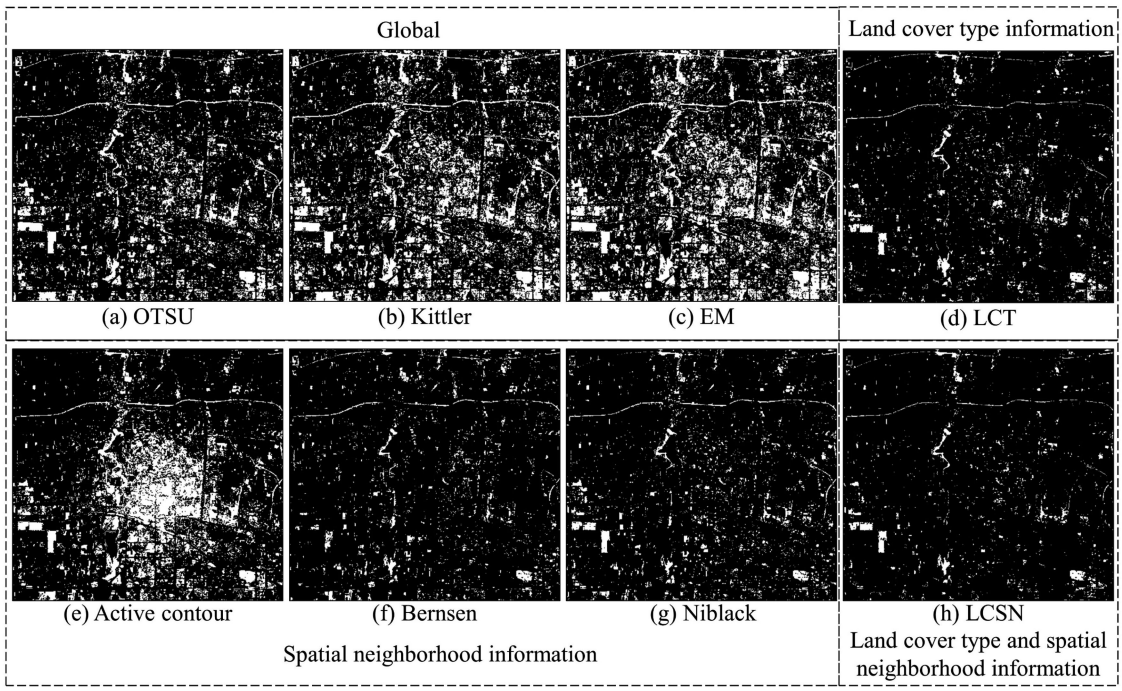

Fig. 5. Change result maps for study area A. (a) OTSU. (b) Kittler. (c) EM. (d) LCT. (e) Active contour. (f) Bernsen. (g) Niblack. (h) LCSN.

information, and the supervised CTS method is based on land cover type information.

1) The LCSN method outperforms the unsupervised CTS method, and the spatial neighborhood information-based local CTS method is superior to the global CTS method. The study area is prone to pseudo changes arising from crop harvesting and phenological differences. As shown in Fig. 7, the unsupervised CTS methods all produce false alarms in red areas, and which the Otsu method, Kittler method, and EM method have higher false alarm rates

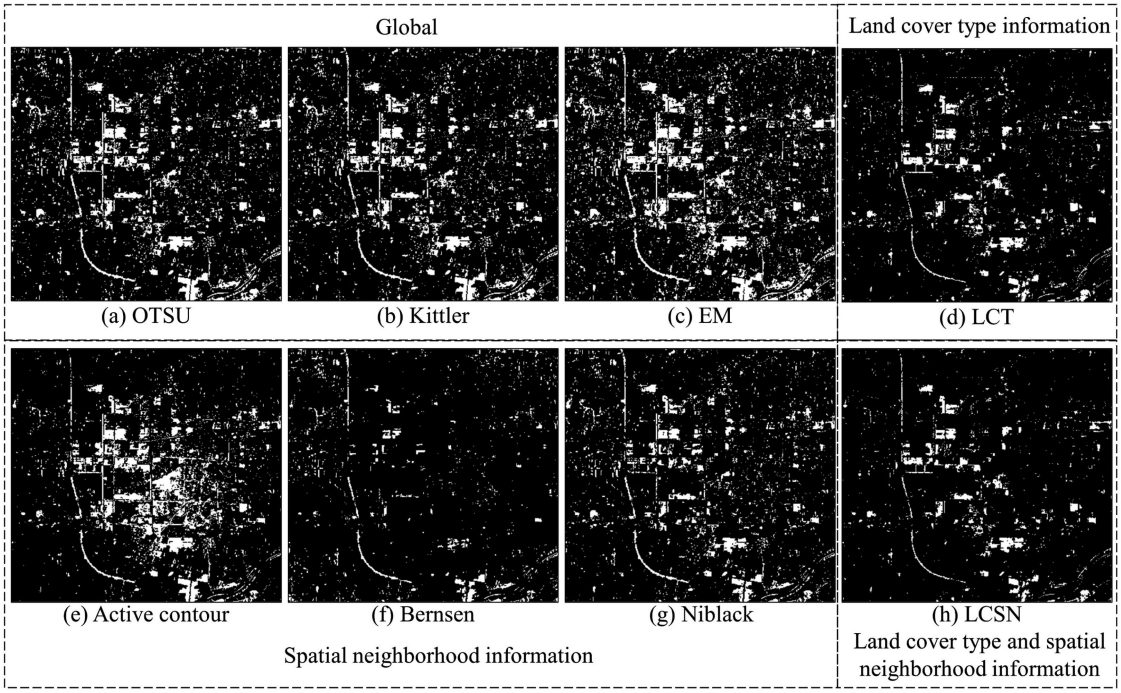

Fig. 6. Change result maps for study area B. (a) OTSU. (b) Kittler. (c) EM. (d) LCT. (e) Active contour. (f) Bernsen. (g) Niblack. (h) LCSN.

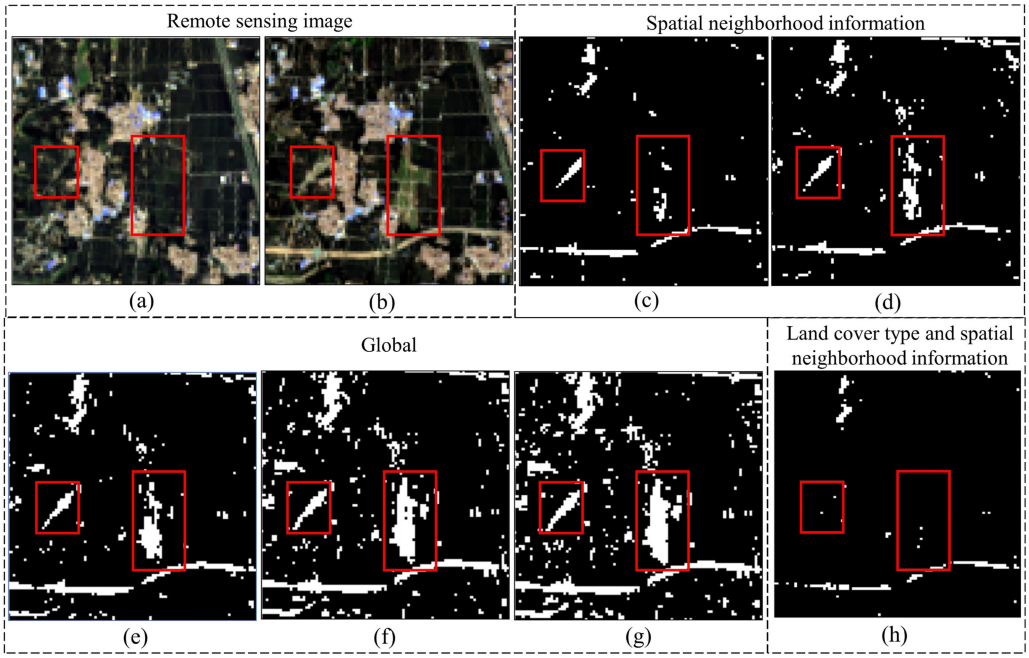

Fig. 7. Comparison of local change detection results. (a) Image at 2013. (b) Image at 2018. (c) Niblack. (d) Bernsen. (e) OTSU. (f) Kittler. (g) EM. (h) LCSN.

than the Niblack method and Bernsen method; false alarms have less frequency with the LCSN method.

2) The detection effect of the LCSN method is better than that of the supervised CTS method. The yellow area in Fig. 8 is the real area of change, and the red area is the pseudo change area. The LCT method and the LCSN method can fully detect the real changes in the yellow area, but the LCT method clearly produces false alarms in the red area. Therefore, the LCSN method is more universal and accurate than the other methods.

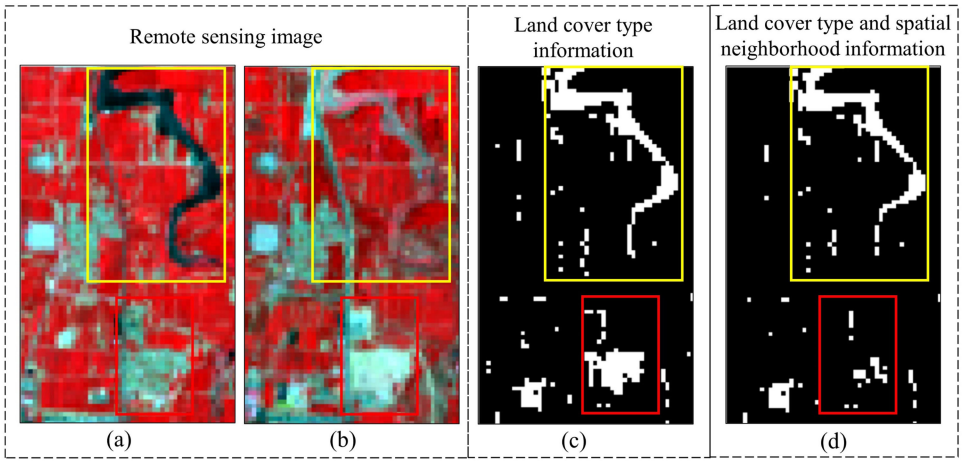

Fig. 8. Comparison of local change detection results. (a) Image at 2013. (b) Image at 2018. (c) LCT. (d) LCSN.

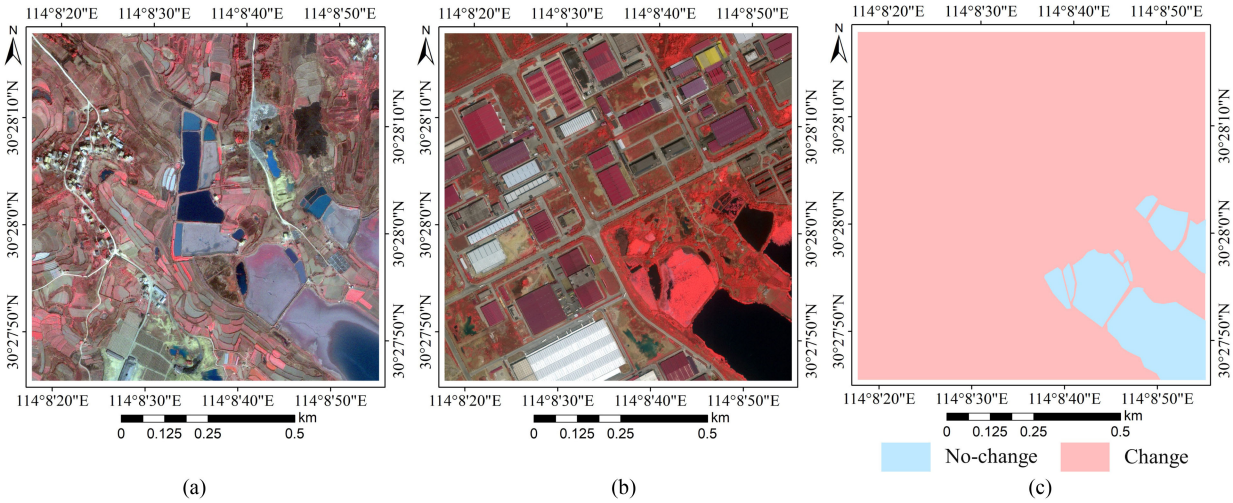

Fig. 9. (a) and (b) Remote sensing images of study area C in 2002 and 2009, respectively. (c) Reference map for study area C.

B. Experiments in Study Area C Using IKONOS Data

Study area C was identified in four bands (red, green, blue, and near-infrared) of IKONOS images with a resolution of 1 m taken on February 11, 2002, and June 24, 2009 [41]. Study area C is located in Hanyang, Wuhan City, China, and the image size is 1000×1000 pixels. Basic image preprocessing (e.g., radiometric calibration, atmospheric correction, and geometric correction) was performed for study area C [42]. As shown in Fig. 9, the types of land cover included in the study area were farmland, water bodies, grassland, woodland, and artificial surfaces.

Study area C underwent changes over the studied period, mainly shifting from agricultural land to building land (e.g., factory sheds), grassland, and woodland. The 48 374 pixel samples that changed and 21 139 pixel samples that did not change were selected for accuracy analysis. The LCSN method yielded the highest OA and F_1-score and relatively low CR and OR values, as shown in Table III. The results in Fig. 10 indicated that both the global CTS method and the spatial neighborhood information-based local CTS method yield unsatisfactory detection results, with obvious misses. The LCT method utilizes land cover type information and provides higher detection accuracy than these two types of CTS methods. The LCSN method, simultaneously accounting for land cover type information and spatial neighborhood information, is excellent in identifying areas of small-magnitude changes in land cover type.

IV. Discussion

A. Accuracy Analysis of the LCSN Method

The LCSN method minimizes the pseudo changes in farmland caused by external factors and detects changes of small magnitude, such as the conversion of farmland to grassland and woodland. To further demonstrate the generality of the LCSN method, a comparative analysis was performed with the global CTS method (the EM method), the spatial neighborhood information-based local CTS method (the Bernsen method), and

TABLE III
COMPARISON OF THE ACCURACY OF THE EIGHT CTS METHODS FOR STUDY AREA C

Method	Unsupervised						Supervised	
	Global			Spatial neighborhood information			Land cover type information	Land cover type and spatial neighborhood information
	OTSU	Kittler	EM	Active contour	Bernsen	Niblack	LCT	**LCSN**
OA (%)	53.89	52.29	52.95	56.39	52.70	51.43	85.62	**92.95**
κ	0.20	0.21	0.22	0.23	0.10	0.20	0.69	**0.84**
CR (%)	10.80	0.01	1.43	9.24	32.84	0.91	1.16	**2.87**
OR (%)	61.54	68.55	66.98	58.62	53.61	69.40	20.15	**8.87**
F_1-score (%)	53.72	47.84	49.41	56.91	57.71	46.72	88.54	**94.73**

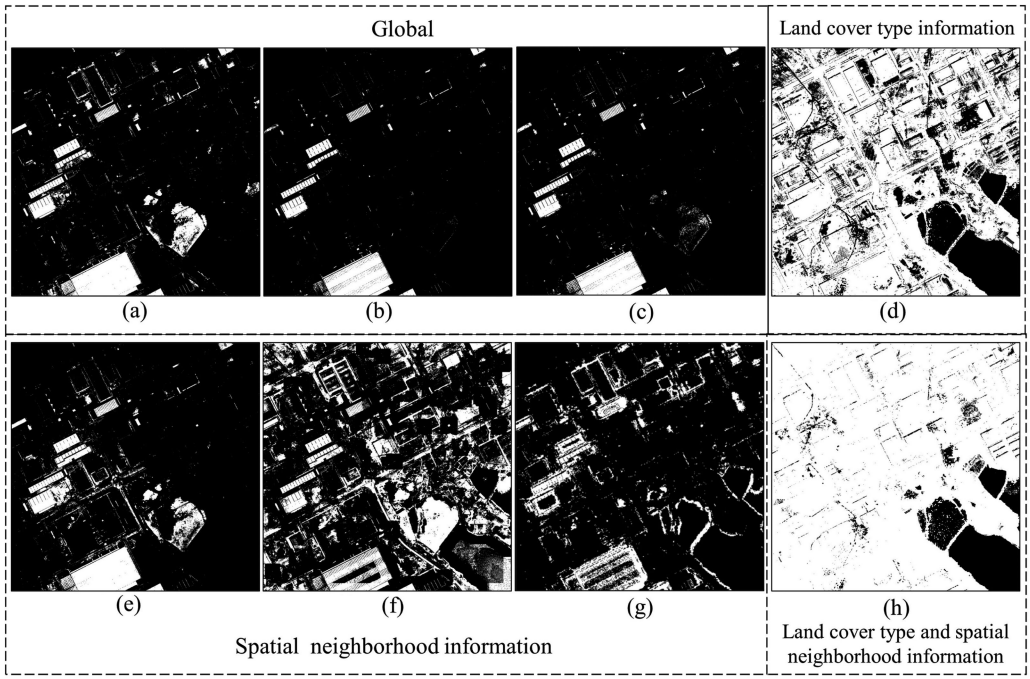

Fig. 10. Change result maps for study area C. (a) OTSU. (b) Kittler. (c) EM. (d) LCT. (e) Active contour. (f) Bernsen. (g) Niblack. (h) LCSN.

the land cover type information-based CTS method (the LTC method).

The results indicate that although floating weeds were present on the water surface, pixel A did not change in 2009 with a grayscale value of 76. Pixel B underwent a change from farmland to grassland with a grayscale value of 23. Pixel C changed from farmland to a factory shed with a grayscale value of 116 (see Fig. 11). The threshold value of 77 determined according to the EM method can be used to detect changes in pixel C, but changes in pixel B are not detected; additionally, no false alarms occur for pixel A. Hence, the global CTS method is likely to miss the detection of changes in different land cover types. This issue is because global CTS is based on the histogram distribution of the corresponding CMM, which only considers grayscale value information and neglects the areas of change with small grayscale values.

The Bernsen method is a local CTS method based on spatial neighborhood information that discovers more areas of change than the EM method. This method only selects the most appropriate threshold within the selected window; although taking this method considers spatial neighborhood information, it still calculates the grayscale value rather than using land cover type information. As shown in Fig. 12, when handling regions with monotonic brightness, the Bernsen method generates strong error noise, resulting in false alarms and missed alarms in some cases [13].

The LCT method is a CTS method based on land cover type information. This method, like the LCSN method, integrates the land cover type information, and the detection result is favorable; however, subtle errors are still found in some areas due to the lack of spatial neighborhood information considered in this method (see Fig. 13). According to the above results, the LCSN method is well suited for detecting the presence of real changes in areas with small grayscale values (e.g., conversion of farmland to grassland) or avoiding pseudo changes with large grayscale values (e.g., presence of floating weeds in water) in the study area.

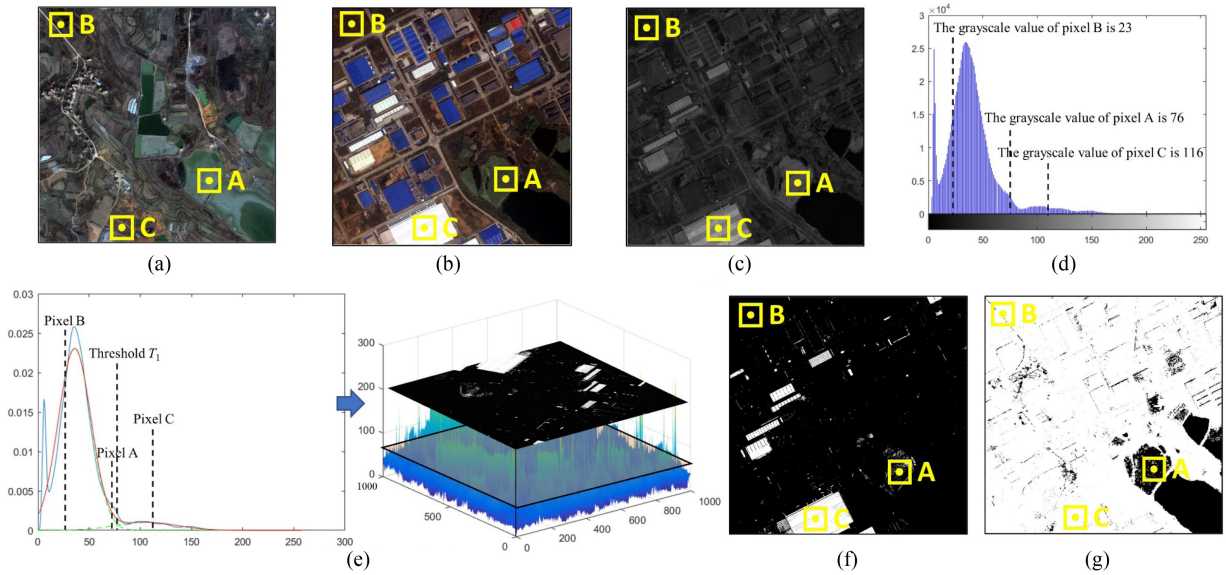

Fig. 11. CTS with the EM method. (a) Image at 2002. (b) Image at 2009. (c) CVA. (d) Grayscale histogram distribution. (e) Global method. (f) EM. (g) LCSN.

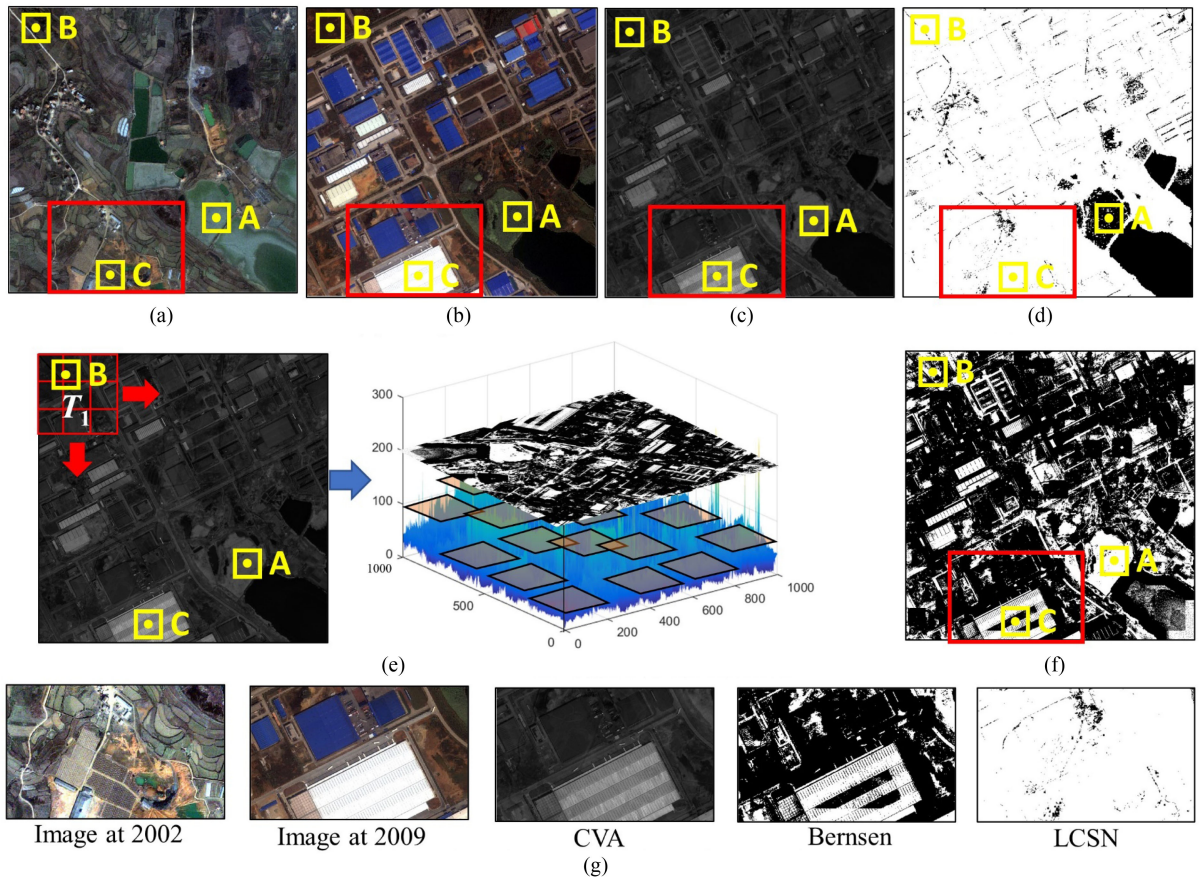

Fig. 12. CTS with the Bernsen method. (a) Image at 2002. (b) Image at 2009. (c) CVA. (d) LCSN. (e) Spatial neighborhood information based local method. (f) Bernsen. (g) Red study area and detection result of image at 2002, image at 2009, CVA, Bernsen, and LCSN.

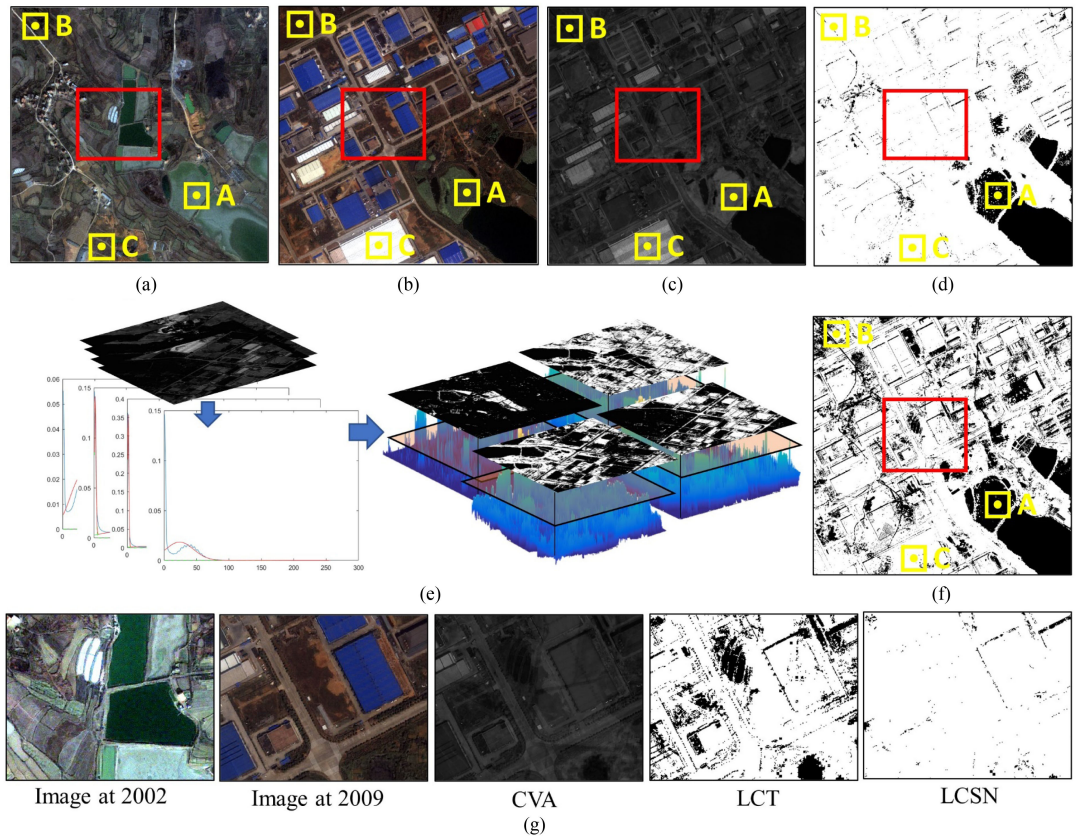

Fig. 13. CTS with the LCT method. (a) Image at 2002. (b) Image at 2009. (c) CVA. (d) LCSN. (e) Land cover type information based method. (f) LCT. (g) Red study area and detection result of image at 2002, image at 2009, CVA, LCT, and LCSN.

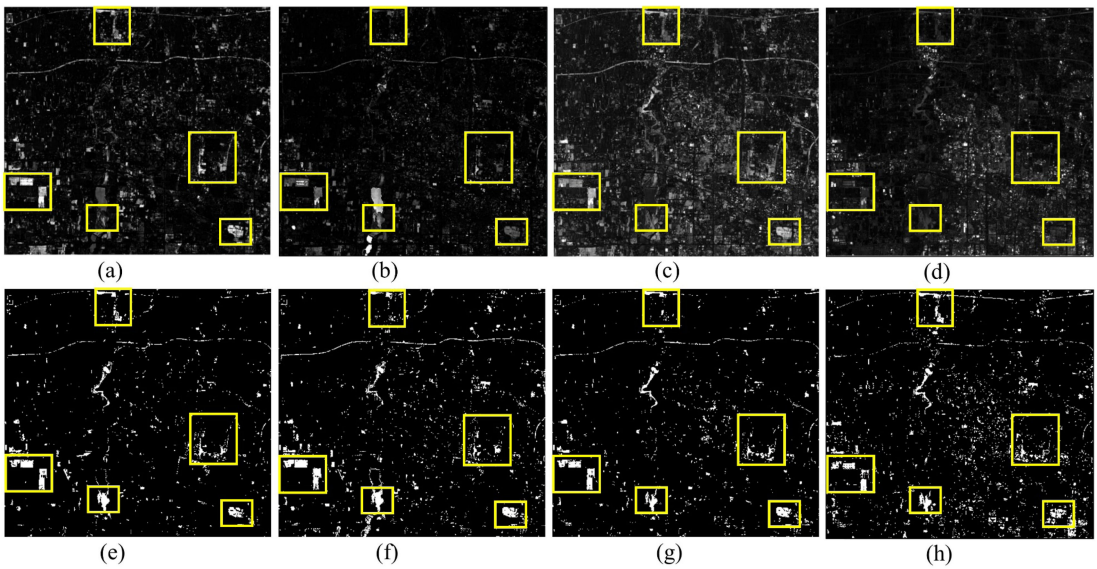

Fig. 14. (a)–(d) CMMs in study area A. (e)–(h) Change result maps for study area A. (a) SAM. (b) SCM. (c) AD. (d) SFA. (e) SAM-LCSN. (f) SCM-LCSN. (g) AD-LCSN. (h) SFA-LCSN.

The LCSN method uses land cover type information to reduce the misclassification of real changes and the identification of pseudo changes. Moreover, spatial neighborhood information is considered to reduce the fine-grained detection results, thereby increasing the accuracy of the detection results.

B. Robustness Analysis of the LCSN Method

To investigate the robustness of the LCSN method, the detection results of different CMMs were investigated. In this article, experiments were conducted using the spectral angle mapper method [43], the spectral correlation mapper method [44], the absolute distance method [18], and the slow feature analysis method [45] for study area A. The detection results are shown in Fig. 14. Notably, the real changes in the yellow areas are obtained with different grayscale values by different CMM methods, but the LCSN method is capable of detecting all these real changes and identifies relatively few pseudo changes. Thus, the LCSN method is robust for use with various CMMs.

V. Conclusion

The LCSN method is an adaptive CTS method based on LCSN. This method adopts a Bayesian criterion to gain land cover type information and the BF method to acquire spatial neighborhood information. The LCSN method offers higher accuracy and stability than the traditional CTS method. Determining thresholds based on land cover type information and spatial neighborhood information eliminates the influence of different spectral value ranges due to different land cover types and compensates for the shortcomings of single and local thresholds.

The feasibility of the LCSN method was demonstrated by conducting experiments on remote sensing images from two different sensors; specifically, Landsat 8-OLI images and IKONOS images were used, and this approach provided a new conceptual application for the CTS method. Compared with those of the other CTS methods, the OA of the LCSN method in study area A improved by 2.13%, that in study area B improved by 2.14%, and that in study area C improved by 7.33%. The excellent performance of the LCSN method is mainly attributed to the dual consideration of land cover type and spatial heterogeneity.

Although the results of the LCSN method are highly satisfactory, this method still has limitations. The detection results of the LCSN method are, to some extent, influenced by the selected training samples when considering land cover type information. A possible future research direction is to weaken the dependence on the training samples and further improve the accuracy of the LCSN method.

Acknowledgment

The authors would like to thank the editors and the anonymous reviewers for their constructive comments and suggestions, which greatly helped to improve the quality of the manuscript.

References

[1] L. Xu, W. Jing, H. Song, and G. Chen, "High-resolution remote sensing image change detection combined with pixel-level and object-level," *IEEE Access*, vol. 7, pp. 78909–78918, Jun. 2019, doi: 10.1109/ACCESS.2019.2922839.

[2] S. Saha, F. Bovolo, and L. Bruzzone, "Unsupervised deep change vector analysis for multiple-change detection in VHR images," *IEEE Trans. Geosci. Remote Sens.*, vol. 57, no. 6, pp. 3677–3693, Jun. 2019.

[3] X. Zhang, P. Xiao, X. Feng, and M. Yuan, "Separate segmentation of multitemporal high-resolution remote sensing images for object-based change detection in urban area," *Remote Sens. Environ.*, vol. 201, pp. 243–255, 2017.

[4] S. I. Cho and S. J. Kang, "Histogram shape-based scene-change detection algorithm," *IEEE Access*, vol. 7, pp. 27662–27667, Feb. 2019, doi: 10.1109/ACCESS.2019.2898889.

[5] R. Touati and M. Mignotte, "An energy-based model encoding nonlocal pairwise pixel interactions for multisensor change detection," *IEEE Trans. Geosci. Remote Sens.*, vol. 56, no. 2, pp. 1046–1058, Feb. 2018.

[6] Z. Zhu, "Change detection using landsat time series: A review of frequencies, preprocessing, algorithms, and applications," *ISPRS J. Photogramm. Remote Sens.*, vol. 130, no. 10, pp. 370–384, 2017.

[7] D. Peng and Y. Zhang, "Object-based change detection from satellite imagery by segmentation optimization and multi-features fusion," *Int. J. Remote Sens.*, vol. 38, no. 13, pp. 3886–3905, 2017.

[8] P. Du, X. Wang, D. Chen, S. Liu, C. Lin, and Y. Meng, "An improved change detection approach using tri-temporal logic-verified change vector analysis," *ISPRS J. Photogramm. Remote Sens.*, vol. 161, no. 12, pp. 278–293, 2020.

[9] H. Liu and L. Zhang, "Adaptive threshold change detection based on type feature for remote sensing image," *J. Remote Sens*, vol. 24, no. 6, pp. 728–738, 2020.

[10] M. Liu, Y. Ke, Q. Yin, X. Chen, and J. Im, "Comparison of five spatio-temporal satellite image fusion models over landscapes with various spatial heterogeneity and temporal variation," *Remote Sens.,* vol. 11, pp. 2612–2639, 2019.

[11] B. V. S. Jansen, C. A. Kolden, H. E. Greaves, and J. U. H. Eitel, "Remote sensing of environment Lidar provides novel insights into the effect of pixel size and grazing intensity on measures of spatial heterogeneity in a native bunchgrass ecosystem," *Remote Sens. Environ.*, vol. 235, 2019, Art. no. 111432.

[12] M. D. Hossain and D. Chen, "Segmentation for object-based image analysis (OBIA): A review of algorithms and challenges from remote sensing perspective," *ISPRS J. Photogramm. Remote Sens.*, vol. 150, pp. 115–134, 2019.

[13] P. A. Cheremkhin and E. A. Kurbatova, "Comparative appraisal of global and local thresholding methods for binarisation of off-axis digital holograms," *Opt. Lasers Eng.*, vol. 115, no. 4, pp. 119–130, 2019.

[14] A. Asokan and J. Anitha, "Change detection techniques for remote sensing applications: A survey," *Earth Sci. Inform.*, vol. 12, no. 2, pp. 1–18, 2019.

[15] N. Otsu, "Threshold selection method from gray-level histograms," *IEEE Trans. Syst., Man, Cybern.*, vol. SMC-9, no. 1, pp. 62–66, Jan. 1979.

[16] J. N. Kapur, P. K. Sahoo, and A. K. C. Wong, "A new method for grey-level picture thresholding using the entropy of the histogram," *Comput. Vision Graph. Image Process.*, vol. 29, no. 3, pp. 273–285, 1985.

[17] J. Kittler, J. Illingworth, and J. Föglein, "Threshold selection based on a simple image statistic," *Comput. Vision Graph. Image Process.*, vol. 30, no. 2, pp. 125–147, 1985.

[18] L. Bruzzone and S. Member, "Automatic analysis of the difference image for unsupervised change detection," *IEEE Trans. Geosci. Remote Sens.*, vol. 38, no. 3, pp. 1171–1182, May 2000.

[19] B. Cui, Y. Zhang, L. Yan, and J. Wei, "Dual-thresholds change detection in GF-3 SAR images," *J. Remote Sens.*, vol. 24, no. 1, pp. 1–10, 2020.

[20] J. Liang and D. Liu, "A local thresholding approach to flood water delineation using Sentinel-1 SAR imagery," *ISPRS J. Photogramm. Remote Sens.*, vol. 159, pp. 53–62, 2020.

[21] M. Hao, M. Tan, and H. Zhang, "A change detection framework by fusing threshold and clustering methods for optical medium resolution remote sensing images," *Eur. J. Remote Sens.*, vol. 52, no. 1, pp. 96–106, 2019.

[22] S. He and L. Schomaker, "DeepOtsu: Document enhancement and binarization using iterative deep learning," *Pattern Recognit.,* vol. 91, pp. 379–390, 2019.

[23] Y. Yang, Y. Li, and Q. Zhao, "Fuzzy threshold optical remote sensing image segmentation with variable class number based on local spatial information," *Acta Autom. Sin.*, pp. 1–12, 2019.

[24] C. Zhang, G. Li, and W. Cui, "A change detection method of remote sensing image based on vector data," *Geomatics Inf. Sci. Wuhan Univ.*, vol. 46, no. 3, pp. 309–317, 2020.
[25] G. Xian, C. Homer, and J. Fry, "Updating the 2001 National land cover database land cover classification to 2006 by using Landsat imagery change detection methods," *Remote Sens. Environ.*, vol. 113, no. 6, pp. 1133–1147, 2009.
[26] E. F. Lambin and A. H. Strahlers, "Change-vector analysis in multitemporal space: A tool to detect and categorize land-cover change processes using high temporal-resolution satellite data," *Remote Sens. Environ.*, vol. 48, no. 2, pp. 231–244, 1994.
[27] T. Hame, I. Heiler, and J. San Miguel-Ayanz, "An unsupervised change detection and recognition system for forestry," *Int. J. Remote Sens.*, vol. 19, no. 6, pp. 1079–1099, 1998.
[28] L. Bruzzone and S. B. Serpico, "An iterative technique for the detection of land-cover transitions in multitemporal remote-sensing images," *IEEE Trans. Geosci. Remote Sens.*, vol. 35, no. 4, pp. 858–867, Jul. 1997.
[29] C. Wu, B. Du, X. Cui, and L. Zhang, "A post-classification change detection method based on iterative slow feature analysis and Bayesian soft fusion," *Remote Sens. Environ.*, vol. 199, pp. 241–255, 2017.
[30] H. Yu, W. Yang, G. Hua, H. Ru, and P. Huang, "Change detection using high resolution remote sensing images based on active learning and Markov random fields," *Remote Sens.,* vol. 9, 2017, Art. no. 1233.
[31] A. P. Tewkesbury, A. J. Comber, N. J. Tate, A. Lamb, and P. F. Fisher, "A critical synthesis of remotely sensed optical image change detection techniques," *Remote Sens. Environ.*, vol. 160, pp. 1–14, 2015.
[32] M. Elad, "On the origin of the bilateral filter and ways to improve it," *IEEE Trans. Image Process.*, vol. 11, no. 10, pp. 1141–1151, Oct. 2002.
[33] Q. Hu, W. Xu, X. Liu, Z. Cai, and J. Cai, "Hyperspectral image classification based on bilateral filter with multispatial domain," *IEEE Geosci. Remote Sens. Lett.*, pp. 1–5, Apr. 2021.
[34] H. Eviatar and R. L. Somorjai, "A fast, simple active contour algorithm for biomedical images," *Pattern Recognit. Lett.*, vol. 17, no. 9, pp. 969–974, 1996.
[35] J. Bernsen, "Dynamic thresholding of gray-level images," in *Proc. Int. Conf. Pattern Recognit.*, 1986, pp. 1251–1255.
[36] W. Niblack, "An introduction to digital image processing," in *An Introduction to Digital Image Processing*, K. Nagwanshi, Ed. Sunnyvale, CA, USA: LAP Lambert Academic Publishing, 1986.
[37] H. Xing, L. Zhu, J. Niu, B. Chen, W. Wang, and D. Hou, "A land cover change detection method combing spectral values and class probabilities," *IEEE Access*, vol. 9, pp. 83727–83739, Jun. 2021, doi: 10.1109/ACCESS.2021.3087206.
[38] H. Xing, L. Zhu, D. Hou, and T. Zhang, "Integrating change magnitude maps of spectrally enhanced multi-features for land cover change detection," *Int. J. Remote Sens.*, vol. 42, no. 11, pp. 4284–4308, 2021.
[39] M. Crowson, R. Hagensieker, and B. Waske, "Mapping land cover change in northern Brazil with limited training data," *Int. J. Appl. Earth Obs. Geoinf.*, vol. 78, pp. 202–214, 2019.
[40] Y. Xie, T. J. Lark, J. F. Brown, and H. K. Gibbs, "Mapping irrigated cropland extent across the conterminous United States at 30 m resolution using a semi-automatic training approach on Google Earth Engine," *ISPRS J. Photogramm. Remote Sens.*, vol. 155, no. 7, pp. 136–149, 2019.
[41] C. Wu, L. Zhang, and B. Du, "Kernel slow feature analysis for scene change detection," *IEEE Trans. Geosci. Remote Sens.*, vol. 55, no. 4, pp. 2367–2384, Apr. 2017.
[42] C. Wu, L. Zhang, and L. Zhang, "A scene change detection framework for multi-temporal very high resolution remote sensing images," *Signal Process.*, vol. 124, pp. 184–197, 2016.
[43] F. A. Kruse *et al.*, "The spectral image processing system (SIPS)-interactive visualization and analysis of imaging spectrometer data," *Remote Sens. Environ.*, vol. 44, no. 2/3, pp. 145–163, 1993.
[44] L. Yan, W. Xia, Z. Zhao, and Y. Wang, "A novel approach to unsupervised change detection based on hybrid spectral difference," *Remote Sens.,* vol. 10, no. 6, pp. 841–862, 2018.
[45] C. Wu, B. Du, and L. Zhang, "Slow feature analysis for change detection in multispectral imagery," *IEEE Trans. Geosci. Remote Sens.*, vol. 52, no. 5, pp. 2858–2874, May 2014.

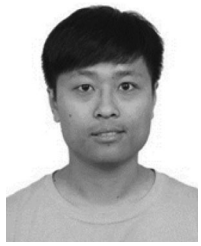

Huaqiao Xing was born in Shandong in 1988. He received the M.S. degree from Beijing University of Architecture, Beijing, China, in 2012, and the Ph.D. degree from China University of Mining and Technology, Beijing, China, in 2017, both in geographic information system (GIS).

After graduation, he joined Shandong Jianzhu University. His main research interests include land cover change detection, geoservice computing, and global discrete grid modeling.

Linye Zhu was born in Wuyishan City, Fujian Province, China, in 1997. She received the BSc. degree in GIS from Shandong Jianzhu University, Jinan, China, where she is currently working toward the M.Eng. degree in surveying and mapping.

Her main research interests are land cover change detection.

Yongyu Feng was born in Shandong in 1979. He received the M.S. degree in geodesy and survey engineering from Henan Polytechnic University, Jiaozuo, China, in 2005.

After graduation, he joined Shandong Institute of Territorial Spatial Data and Remote Sensing Technology. His main research include information construction of natural resources.

Wei Wang was born in Anji, Zhejiang Province, in 1974. She received the Ph.D. degree in geographic information system from the Institute of Geographical Sciences and Resources, Chinese Academy of Sciences, Beijing, China, in 2006.

She is currently an Associate Researcher with the National Center for Disaster Reduction, Ministry of Civil Affairs. She is mainly engaged in the research of disaster remote sensing application.

Dongyang Hou was born in 1986. He received the Ph.D. degree in geographic information system from the China University of Mining and Technology, Beijing, China, in 2016.

From 2016 to 2019, he was a Lecturer with the College of Geography and Environment, Shandong Normal University, Jinan, China. He is currently a Lecturer with the School of Geosciences and Info-Physics, Central South University, Changsha, China. His main research interests include spatial–temporal data crawling, mining, GIS software development, and remote sensing image retrieval. He is a Secretary for the International Society for Photogrammetry and Remote Sensing Inter Commission Working Group IV/III.

Fei Meng was born in Shandong, China, in 1974. He received the M.S. degree in physical geography from Lanzhou University, Lanzhou, China, in 2002, and the Ph.D. degree in physical geography from East China Normal University, Shanghai, China.

His Main research interests include land cover change and environmental remote sensing.

Yuanlong Ni was born in Shandong, China, in 1987. He received the M.S. degree in GIS from the Institute of Soil Science, Chinese Academy of Sciences, Nanjing, China, in 2012.

His main research interests include the applications of GIS in natural resource management.